Project funded by the European Commission under the 6th (EC) RTD Framework Programme (2002- 2006) within the framework of the specific research and technological development programme “Integrating and strengthening the European Research Area”

Project UpWind

Contract No.:
019945 (SES6)

“Integrated Wind Turbine Design”

SEM in-situ laboratory investigations on damage growth in GFRP composite under three-point bending tests

AUTHOR:	Hongwei ZHOU
AFFILIATION:	China University of Mining and Technology (Beijing)
ADDRESS:	Xueyuan Road D11, Beijing 100083, P. R. China
TEL.:	+86 10 62331286
EMAIL:	zhw@cumtb.edu.cn
FURTHER AUTHORS:	L. Mishnaevsky Jr., P. Brøndsted, J. B. Tan, L. L. Gui
REVIEWER:	
APPROVER:	

Document Information

DOCUMENT TYPE	
DOCUMENT NAME:	SEM in-situ laboratory investigations on damage growth in GFRP composite under three-point bending tests
REVISION:	
REV.DATE:	
CLASSIFICATION:	R1: Restricted to project members
STATUS:	

Abstract: Glass fiber-reinforced polymer (GFRP) composites are widely used in low-weight constructions. SEM (Scanning Electron Microscopy) in-situ experiments of damage growth in GFRP composite under three-point bending loads are carried out. By summarizing the experimental results of three groups of samples with different orientation angles of fibers, the dependence of mechanical parameters on the orientation angles of fibers are analysed. The regression analysis show that the peak strengths, the elastic strengths and the elastic modulus of the composites decease with the orientation angles of fibers almost linearly. Moreover, the damage growth and meso-scale structure changes in GFRP composites during three-point bending loading are analyzed in the paper.

Contents

STATUS, CONFIDENTIALITY AND ACCESSIBILITY									
Status				**Confidentiality**				**Accessibility**	
S0	Approved/Released			**R0**	General public			Private web site	
S1	Reviewed			**R1**	Restricted to project members	**R1**		Public web site	
S2	Pending for review			**R2**	Restricted to European. Commission			Paper copy	
S3	Draft for commends			**R3**	Restricted to WP members + PL				
S4	Under preparation			**R4**	Restricted to Task members +WPL+PL				

PL: *Project leader* **WPL:** *Work package leader* **TL:** *Task leader*

Background

An increasing effort has been directed toward wind power technology in last decades. European Commission through the 6th Framework Programme Grant UpWind focuses on future wind power technology and will develop substantially improved models of the principles wind turbine components, which the industry needs for the design and manufacture of very large scale wind turbines (>8-10MW and rotor diameter>120m), both on- and off-shore. One of the challenges inherent in the creation of such power stations necessitate the advanced materials with extreme strength to mass rations. Glass fiber-reinforced polymer (GFRP) composite, as a kind of material with high ratio of strength to mass, has been used widely in wind turbine blade.

GFRP composites are characterized by high strength and low weight. An important parameter of the composites is their strength and damage resistance at mechanical, static and fatigue loading, both in longitudinal and transverse directions and at different angles to the fiber axes. The strength and damage mechanisms of the composites are strongly influenced by the type and conditions of loadings. So, under longitudinal tensile loading, the main part of the load is born by the fibers, and they tend to fail first in metal and polymer matrix composites. After weakest fibers fail, the load on remaining intact fibers increases. That may cause the failure of other, first of all, neighbouring fibers. According to Cooper (1971), the mechanisms of failure of the composites at this stage can be classified into “single fracture” (after one phase fails, another phase can not bear any load and fails instantly) and “multiple fractures” mechanisms (after one component fails, other components can bear the applied load, but becomes progressively damaged and ultimately fail). In the case of multiple failures, the stress-strain curve looks similar to the ductile stress-strain curve, with a zigzag-like part, corresponding to the stage of accumulation of the cracks before failure [1].

The cracks in the fibers cause higher stress concentration in the matrix, what can lead to the matrix cracking. However, if the fiber/matrix interface is weak, the crack will extend and grow along the interface. The crack deviation into the interfaces may be beneficial for the fracture toughness of composites [2]. In the case of brittle matrix composites (for instance, epoxy might be classified as such in many cases), the crack is formed initially in the matrix. If intact fibers are available behind the crack front and they are connecting the crack faces, the crack bridging mechanism is operative. In this case, the load is shared by the bridging fibers and crack tip, and the stress intensity factor on the crack tip is reduced. A higher amount of bringing fibers leads to the lower stress intensity factor on the crack tip, and the resistance to crack growth increases with increasing the crack length [3,4]. The extension of a crack, bridged by intact fibers, leads to the debonding and pull out of fibers that increase the fracture toughness of the material. The compressive strength of composites is often sufficiently lower than their tensile strength [5]. Failure of the polymer matrix composites is caused usually by localized buckling or kinking of fibers. Further, fiber crushing and shear banding can be observed in the composites under compressive loading [6]. Under tensile loading at an angle to the fiber direction, several failure mechanisms are operative: tensile fiber failure (operative at low angles between the interface and applied force), shear along the interface, tensile interface debonding and matrix cracking (the latter two mechanisms are observed at high angles between the interface and applied force) [7].

The purpose of this study is to analyze and to clarify experimentally the mechanisms of damage growth in the GFRP composites under three-point bending, especially the dependence of strength, modulus, stiffness of the GFRP composite and crack propagation on the orientation angles of unidirectional fibers.

1. Description of Laboratory Experiment

1.1 Materials and dimensions of specimens

The specimens in the report named laminates GF / UD (4 layers, lay-up (90/0 - 0/90 - 90/0)S, fibres PPG 2002) were provided by the Knowledge Centre of Wind Turbine Materials and Constructions (WMC), the Netherlands. The specifications of these materials are as follows: identification number 595/c, system resin RIM 135, system hardener RIM/H 134/137, system

mix ratio 100/30, vacuum curing 1000, post-cure 10hrs at 70ºC, material density 1940,79, Saertex weaver, curing tabs glue 2hrs at 65ºC.

All the GFRP composite specimens were prepared by water jet technology. In order to investigate the influence of fiber orientation angles on the mechanical behaviour of composite materials, the fibers were arranged at different orientation angles with respect to horizontal direction such as 0^0, 15^0, 30^0, 45^0, 60^0, 75^0, and 90^0, respectively (Fig. 1). 3 specimens were prepared for each orientation angle. In another word, there are 21 specimens in total, divided into 3 groups (Table 1).

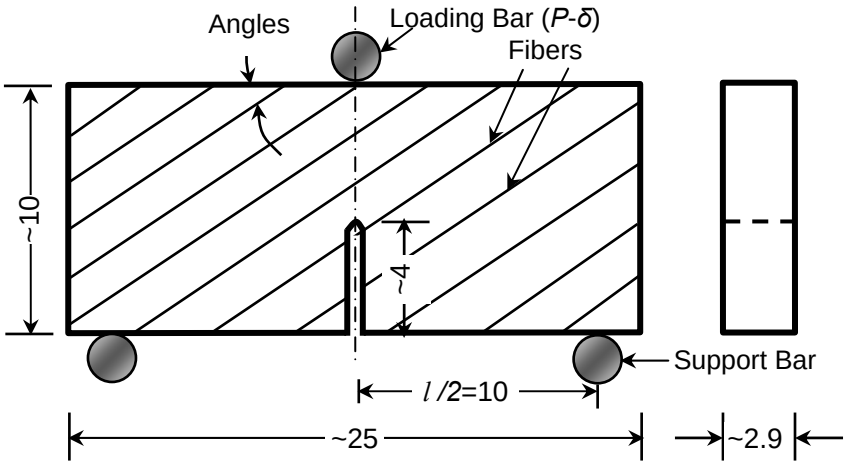

Figure 1 *Dimensions of specimens for three-point bending tests (unit: mm).*

Table 1 Identification numbers of specimens and their dimensions (unit: mm)

Specimen ID	*L*	*H*	*h*	*W*	Specimen view
T-S-0^0-1/2/3	24.7/24.5/24.5	8.8/8.9/8.8	3.4/3.4/3.5	2.9/2.9/2.9	
T-S-15^0-1/2/3	24.7/24.5/24.6	8.9/9.2/9.3	3.7/3.7/3.7	2.9/2.9/2.9	
T-S-30^0-1/2/3	24.8/24.7/24.7	8.7/8.8/8.9	3.1/3.5/3.3	2.9/2.9/2.9	
T-S-45^0-1/2/3	24.2/24.0/24.3	8.8/8.8/8.8	3.2/3.1/3.6	2.9/2.9/2.9	
T-S-60^0-1/2/3	24.8/24.7/24.6	9.1/9.2/8.8	4.0/3.7/3.7	2.9/2.9/2.9	
T-S-75^0-1/2/3	24.7/24.6/24.6	9.2/9.3/9.0	3.3/3.5/3.2	2.9/2.9/2.9	
T-S-90^0-1/2/3	24.5/24.7/24.7	9.7/9.1/9.1	3.6/3.7/3.7	2.9/2.9/2.9	

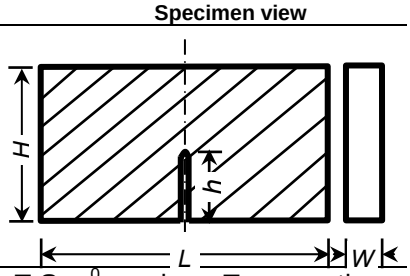

Note: The identification number of specimens was defined as **T**-**S**-**m**^{0}-**n**, where **T** means three-point bending, **S** means static, **m** means orientation angles of fibers with respect to horizontal direction, and **n** means the group number of specimens (in the present study **m**=0, 15, 30, 45, 60, 75, 90, **n**=1, 2, 3).

1.2 Test System

All the tests were carried out with the use of the SEM fatigue testing system, developed and provided by *Shimadzu Co., Japan, and available at China University of Mining and Technology (Beijing)*. The system is used for a real time in-situ observation of the meso- and micro-scale structural changes and the flaw evolution of the metal and non-metal materials which are subjected to static or dynamic loads. The system is controlled by the full digital servo hydraulic control, allows the loading up to ±10KN, load frequency: 0.00001~10Hz (which may be extended to 100Hz if one uses very small stroke range), and temperature from room temperature up to 800^0C. Different loading modes can be employed: tensile, compression and three-point bending. Other parameters are as follows: Magnification: 35~200,000 times, Scanning speed: 0.27s/f~9.6s/f, Observation resolution: 5.5 nm (low vacuum) and 3.5 nm (high vacuum).

1.3 Experimental Procedure

The specimens of GFRP composite were immerged into beaker containing pure alcohol, and then washed for 1-2 minutes using the ultrasonic device. After the volatilization of the alcohol on the specimen surface, A hydronium sputtering instrument (Type: KYKY SBC-12) was employed to gild the specimens for 330 seconds to obtain secondary electron and therefore improve the quality of real-time observation.

The GFRP composite specimen was fixed on the platform of the loading cell for three-point bending test, which was then inserted into the SEM chamber. It should be stressed that the prefabricated notch in a specimen should be right under the loading bar (Figure 1). Vacuum was created so that the surface image of sample can be captured clearly. The SEM was adjusted to obtain an SEM image with appropriate brightness and contrast, and one should focus on the pre-existing notches at the centre of the sample in order to catch the process of crack development. A displacement-controlled load was applied to the sample with a loading rate of 1.5×10^{-3} mm/s until the sample fails. During loading, displacements (here means the deflection of a specimen) and loads were recorded automatically by the test system. Additionally, SEM photos were taken at any moments when changes of meso-scale structure or damage growth occurred in the specimen.

2. Experimental Results and Analysis

2.1 Experimental Results

(1) Group 1

Seven specimens in this group were identified by **T**-**S**-**m**^{0}-**1** (here m=0, 15, 30, 45, 60, 75, 90). The load-deflection relations of the three-point bending beam (*P-δ* curves) given by the test system are shown in Figure 2(a). Figure 4(b) shows the failure mode of specimens after loading.

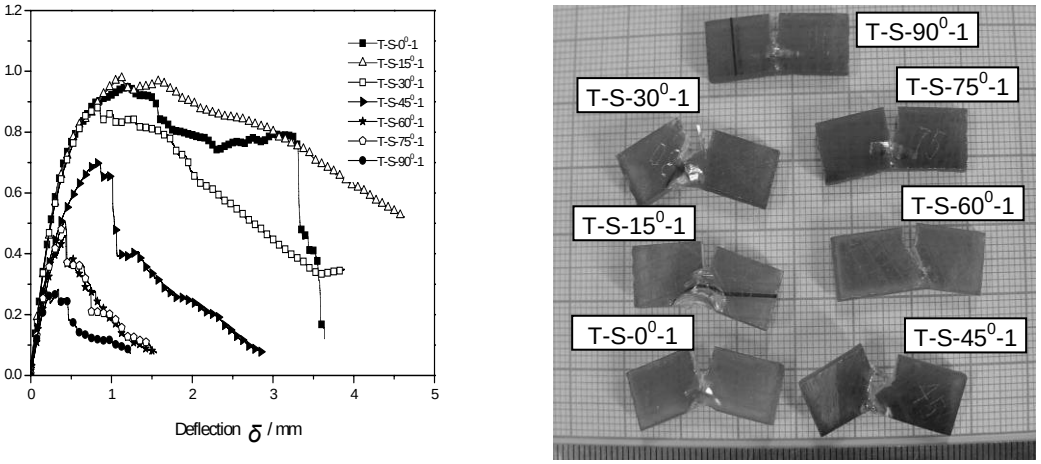

(a) (b)

Figure 2 *P-δ curve of Group 1 specimens (a) and their failure mode (b)*.

(2) Group 2

Seven specimens in Group 2 were identified by **T**-**S**-**m**^{0}-**2** (here m=0, 15, 30, 45, 60, 75, 90). The *P-δ* curves given by the test system are shown in Figure 3(a). Figure 5(b) shows the failure mode of specimens after loading.

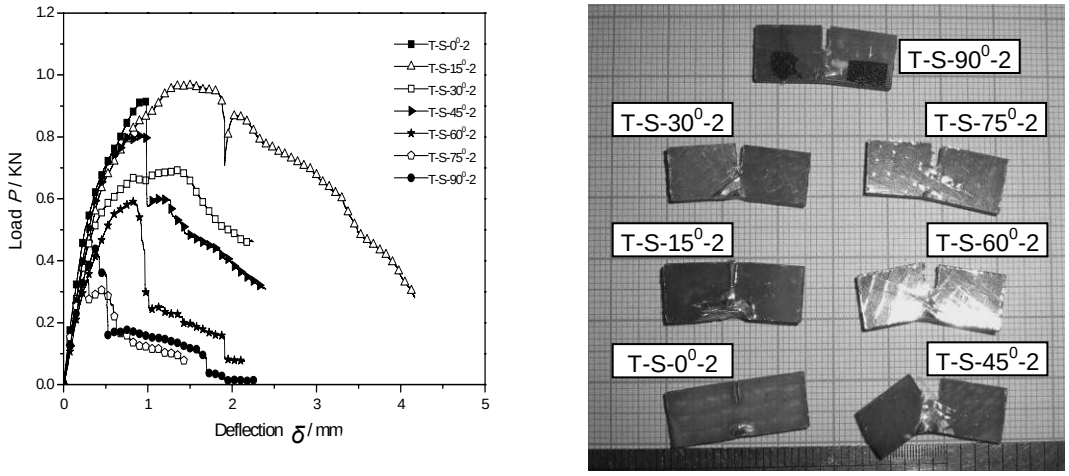

(a) (b)

Figure 3 *P-δ curve of Group 2 specimens (a) and the* failure mode *(b)*.

(3) Group 3

Seven specimens in this group were identified by **T-S-m^0-3** (here m=0, 15, 30, 45, 60, 75, 90). The *P-δ* curves given by the test system are shown in Figure 4(a). Figure 6(b) shows the failure mode of specimens after loading.

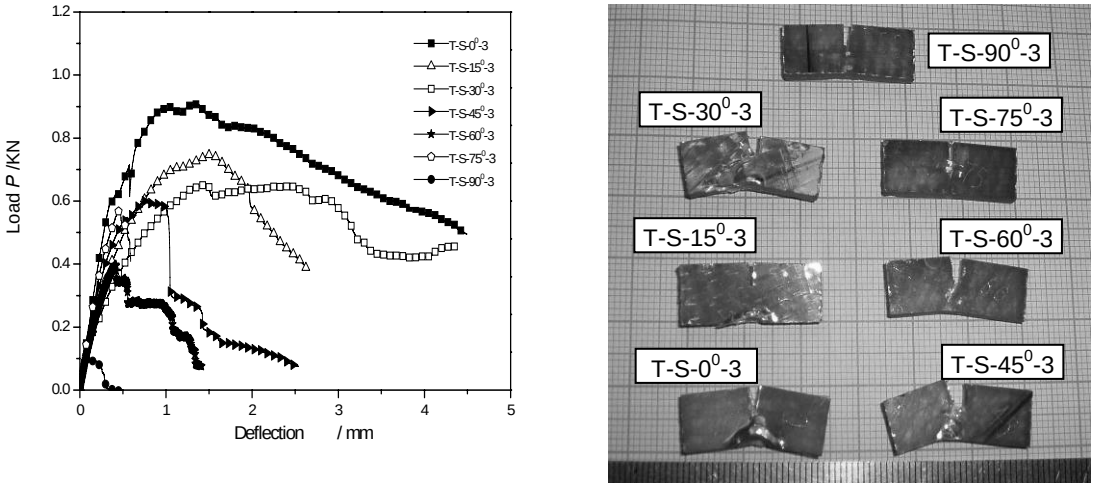

(a) (b)

Figure 4 *P-δ curve of Group 3 specimens (a) and the* failure mode *(b)*.

2.2 Dependence of Strength and Modulus on Orientation Angles of Fibers

(1) Peak Strength

According to three-point bending beam method, the peak strength of three-point bending beam is given by

$$\sigma_p = \frac{P_{\max} l(H-h)}{8I} \tag{1}$$

where P_{max} is the maximum value of applied load (Figure 7). I is the inertial moment of the effective cross-sectional area, $I = W(H-h)^3/12$, *W*, *H*, *h* are available in Table 1. l is the span between support bars (Figure 1), l=20mm.

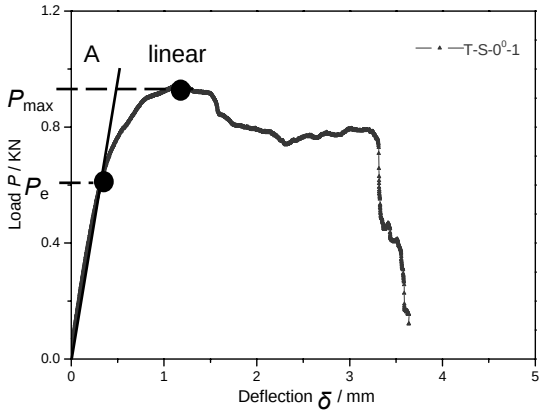

Figure 5 *Schematic view of a maximum elastic load P_e and peak load P_{max} in a P-δ curve*.

The peak strengths of GFRP composite are calculated by Eq. (1). Figure 6a shows that the peak strengths decrease with orientation angles of fibers. However, it is of interest that, Specimens T-S-15^0-1 and T-S-15^0-2 appear to have even higher strength than those with fibers ideally perpendicular to the loading direction. By averaging the peak strengths for the specimen with the same orientation angles of fibers, one may get a regression relation between the average peak strength $\overline{\sigma}_p$ and the orientation angles of fibers θ (as shown in Figure 6b)

$$\overline{\sigma}_p = 336.69 - 2.47\theta \tag{2}$$

where $\overline{\sigma}_p$ is the average peak strength in MPa, θ is the orientation angle of fibers in degree.

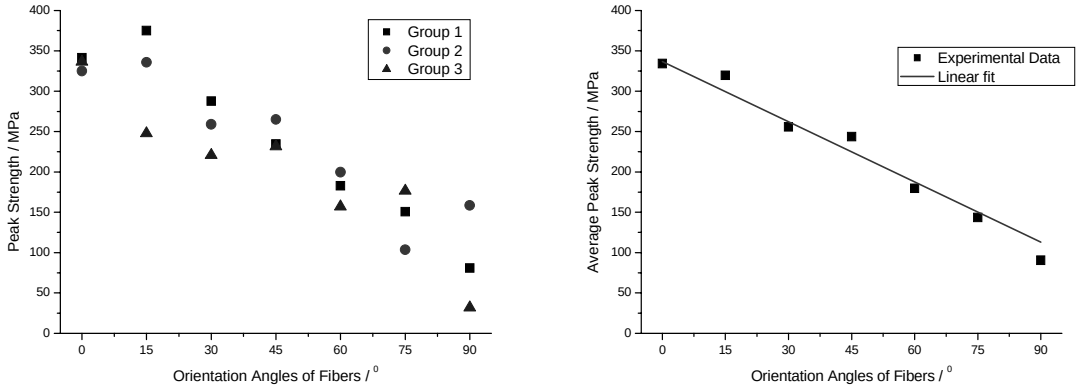

(a) (b)

Figure 6 *Correlations between peak strengths (a), average peak strengths (b) and orientation angles of fibers*.

(2) Elastic Strength

The elastic strength for three-point bending beam is given by

$$\sigma_e = \frac{P_e l(H-h)}{8I} \tag{3}$$

where P_e is the maximum elastic value of applied load, determined by a data point of departure from a linear line in a *P-δ* curve (Figure 5).

Eq.(3) is used to calculate the elastic strengths of composite materials (Figure 7a). By averaging the elastic strengths (Figure 7b), one may again get a regression relation as

$$\overline{\sigma}_e = 167.80 - 1.07\theta \tag{4}$$

where $\overline{\sigma}_e$ is the average elastic strength in MPa, θ is the orientation angle of fibers in degree.

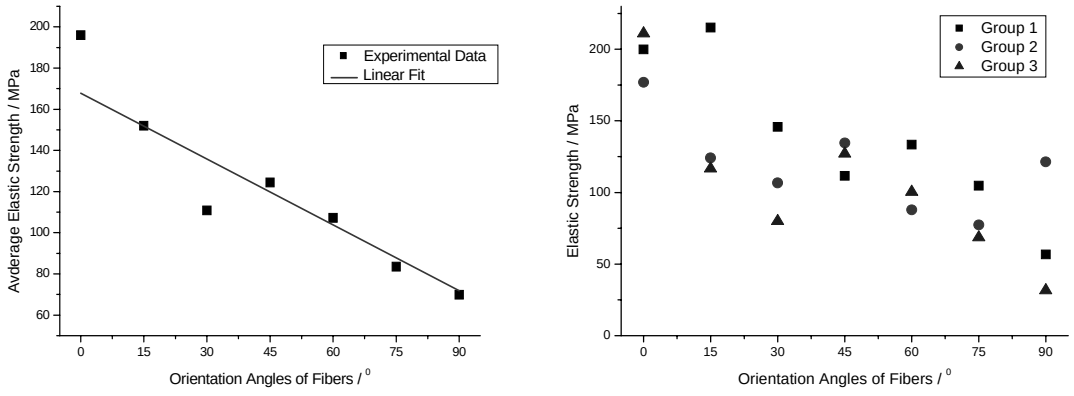

(a) (b)

Figure 7 *Correlations between elastic strengths (a), average elastic strengths (b) and orientation angles of fibers*.

(3) Elastic Modulus

The deflection of the three-point bending beam is given by

$$\delta = \frac{P_e l^3}{48EI} \tag{5}$$

where *E* is elastic modulus.

A slope of a linear fit of *P-δ* curve is given by

$$k = \frac{\sum_{i=1}^{n} P_i \cdot \sum_{i=1}^{n} \delta_i - n\sum_{i=1}^{n} P_i\delta_i}{(\sum_{i=1}^{n} P_i)^2 - n\sum_{i=1}^{n} P_i^2} \tag{6}$$

where *n* is the number of data points in the linear stage of *P-δ* curves. Then the elastic modulus are given by

$$E = \frac{l^3}{4kW(H-h)^3} \tag{7}$$

The elastic modulus can be estimated by Eq. (7) (Figure 8a). It is indicated that, in general, the elastic modulus decreased with the orientation angles of fibers. Again, by averaging the elastic modulus at the same orientation angles of fibers (Figure 8b), one may get a regression equation of average elastic modulus

$$\overline{E} = 8146.53 - 34.22\theta \tag{8}$$

where $\overline{E}$ is the average elastic strength in MPa, θ is the orientation angle of fibers in degree.

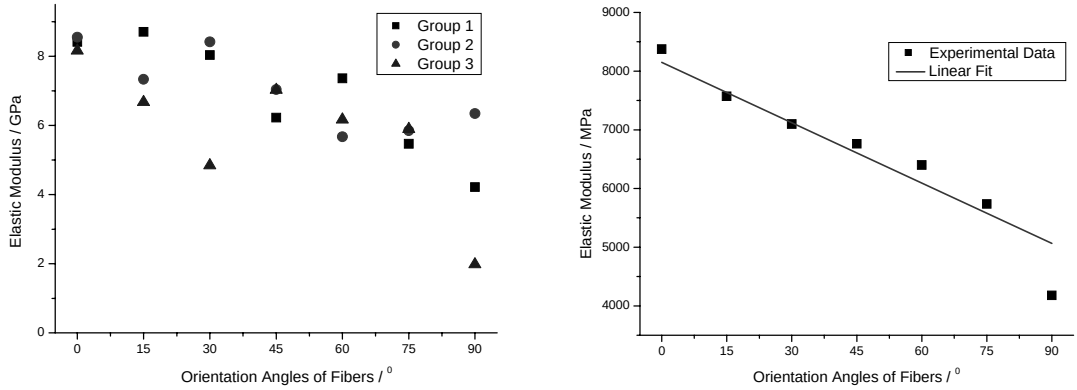

(a) (b)

Figure 8 *Correlations between elastic modulus (a), average elastic modulus (b) and orientation angles of fibers*.

3. Damage Growth during Three-point Bending

The SEM testing system can record automatically the *P-δ* curves (Figures 2a, 3a and 4a), at the same time, SEM photos can be taken at any given load in order to indicate the damage growth and change of the meso-scale structures of the samples during three-point bending loading. Figure 9 shows *P-δ* curves and their corresponding SEM photos.

3.1 General Behaviour of Damage Growth in GFPP Composite

Figure 9 shows that the meso-scale structures of composite almost remain unchanged before peak loads, namely no damage occurs at the tip of the pre-existing notch. However, a continuous loading near the peak strength leads to a matrix cracking first, and the interface between the matrix and the fiber breaks then. As shown in Figure 11, a typical process of damage growth in GFRP composite can be described as follows: with a continuous loading, a crack is formed in the matrix first in the vicinity of peak strength; then, a crack occurs at the interface between the matrix and the fiber. At the moment, the composite still has a residual load-bearing capability. The damage growth and cracking formation in GFRP composite appear to be dependent on the orientation angles of fibers.

As shown in Figures 6, 7 and 8, the orientation angles of fibers have a significant effect on mechanical parameters of GFRP composite such as strength and elastic modulus. In addition, the orientation angles of fibers also play an important role in stiffness of GFRP composite (Figures 2a, 3a and 4a). A lower orientation angle of fibers ensures a higher strength and stiffness, indicating a better harmonic load-bearing capability of both matrix and fibers before peak strength. The GFRP composite appears to be obviously anisotropic. The *P-δ* curves are similar with the evolution of meso-scale damage in GFRP composite, indicating a dependence of both mechanical parameters and damage growth on the orientation angles of fibers.

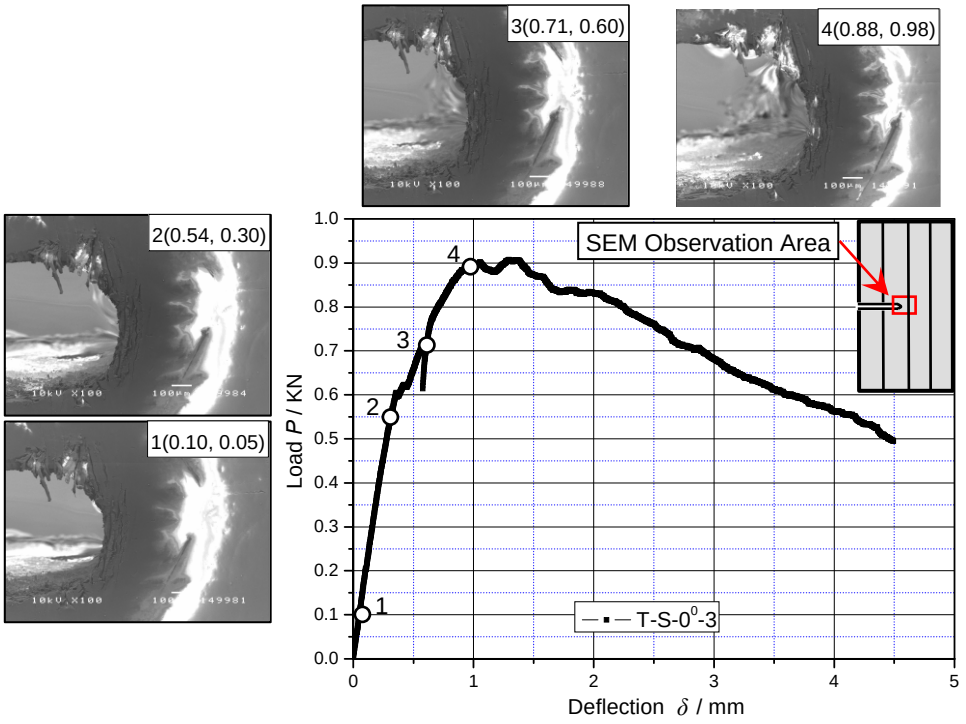
3(0.71, 0.60)
4(0.88, 0.98)
2(0.54, 0.30)
1(0.10, 0.05)
SEM Observation Area
Load P / KN
Deflection δ / mm
T-S-0⁰-3
1
2
3
4

(a)

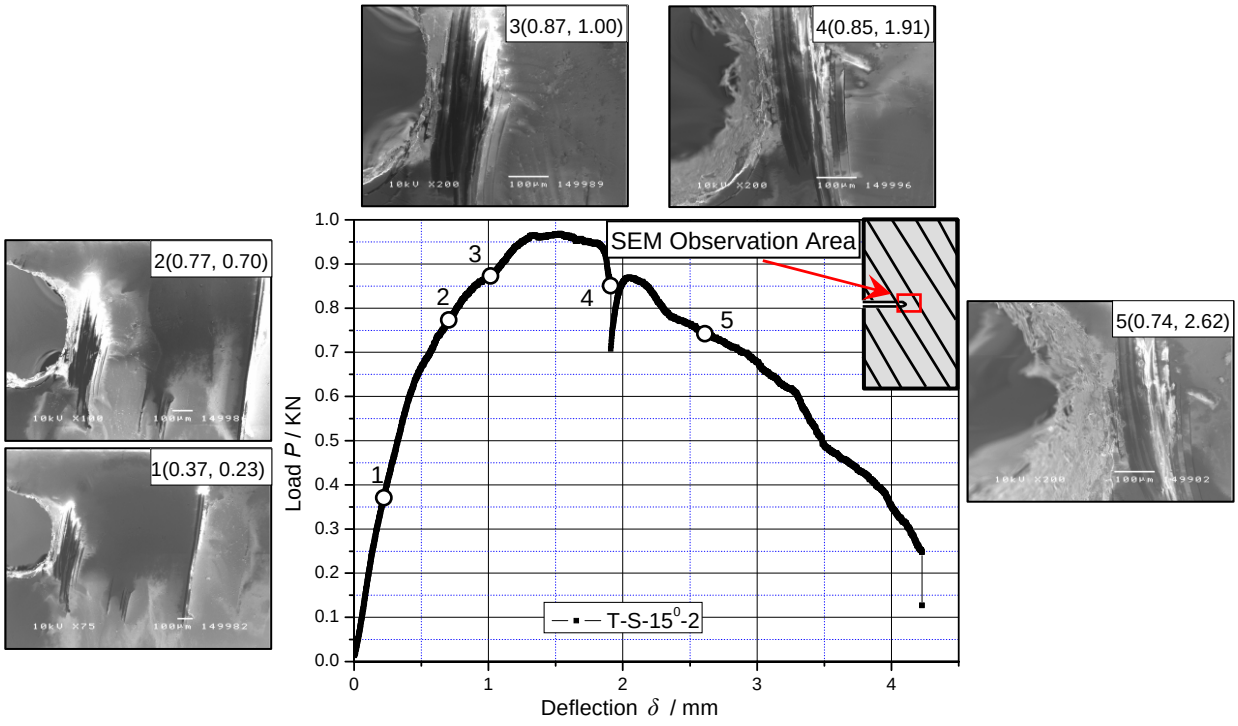
3(0.87, 1.00)
4(0.85, 1.91)
2(0.77, 0.70)
1(0.37, 0.23)
5(0.74, 2.62)
SEM Observation Area
Load P / KN
Deflection δ / mm
T-S-15⁰-2
1
2
3
4
5

(b)

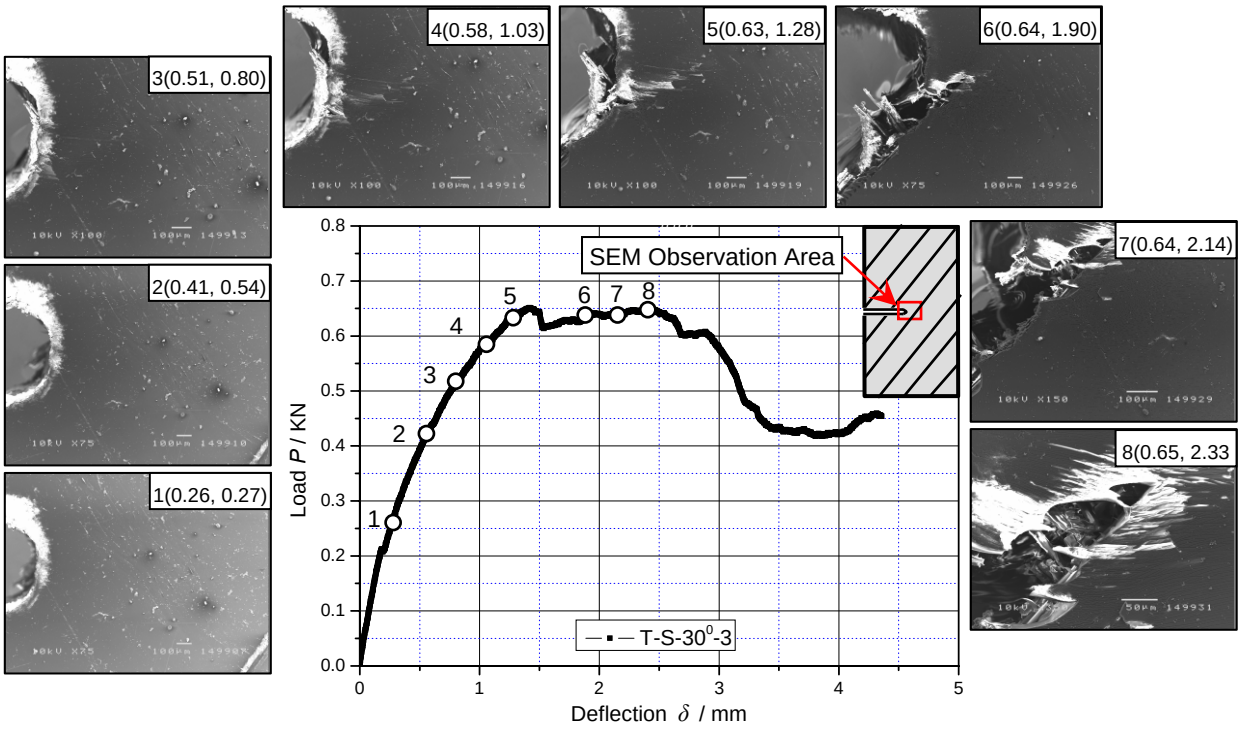
3(0.51, 0.80)
4(0.58, 1.03)
5(0.63, 1.28)
6(0.64, 1.90)
2(0.41, 0.54)
1(0.26, 0.27)
SEM Observation Area
7(0.64, 2.14)
8(0.65, 2.33)
Load P / KN
Deflection δ / mm
T-S-30°-3

(c)

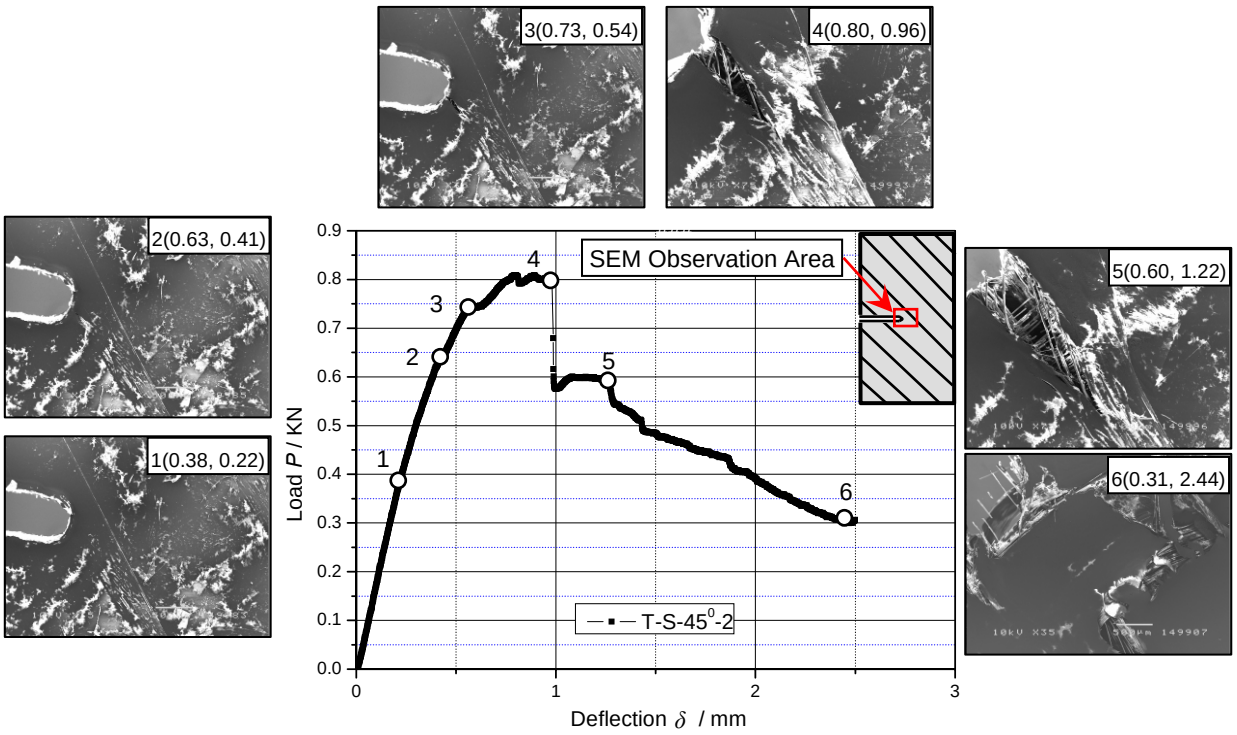
3(0.73, 0.54)
4(0.80, 0.96)
2(0.63, 0.41)
1(0.38, 0.22)
SEM Observation Area
5(0.60, 1.22)
6(0.31, 2.44)
Load P / KN
Deflection δ / mm
T-S-45°-2

(d)

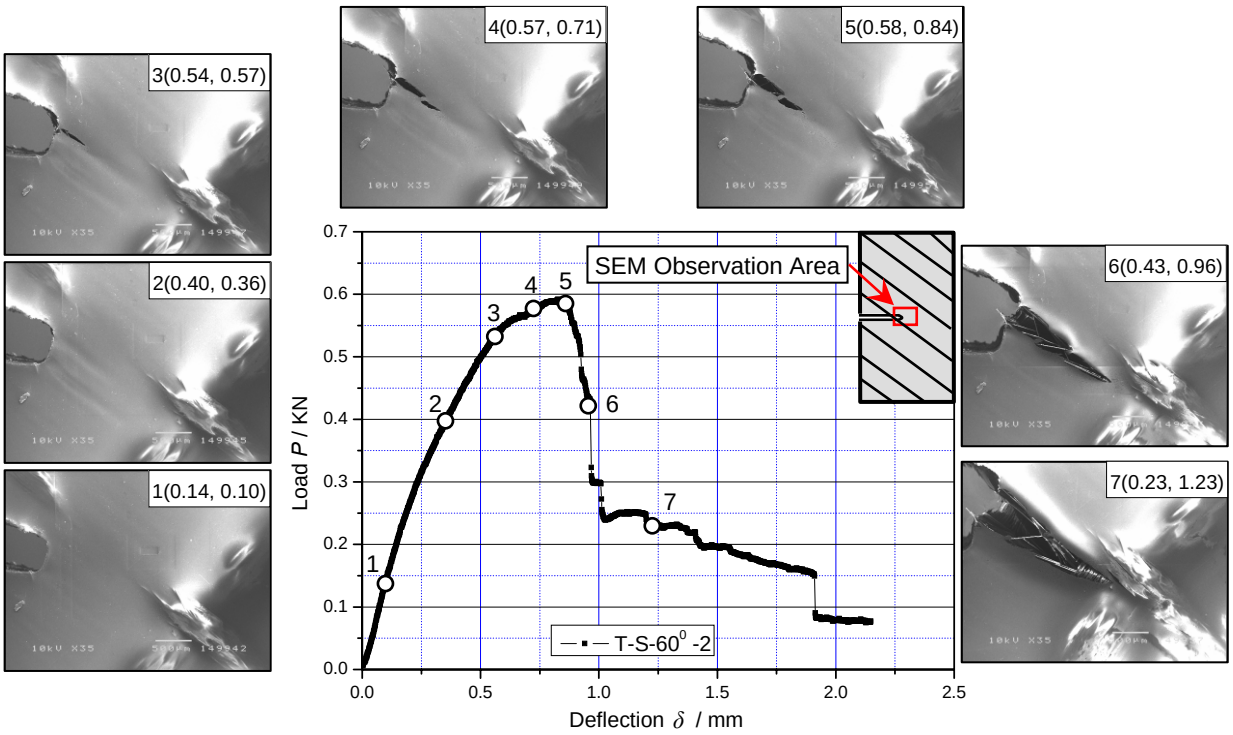
3(0.54, 0.57)
4(0.57, 0.71)
5(0.58, 0.84)
2(0.40, 0.36)
1(0.14, 0.10)
SEM Observation Area
6(0.43, 0.96)
7(0.23, 1.23)
Load P / KN
Deflection δ / mm
T-S-60⁰ -2

(e)

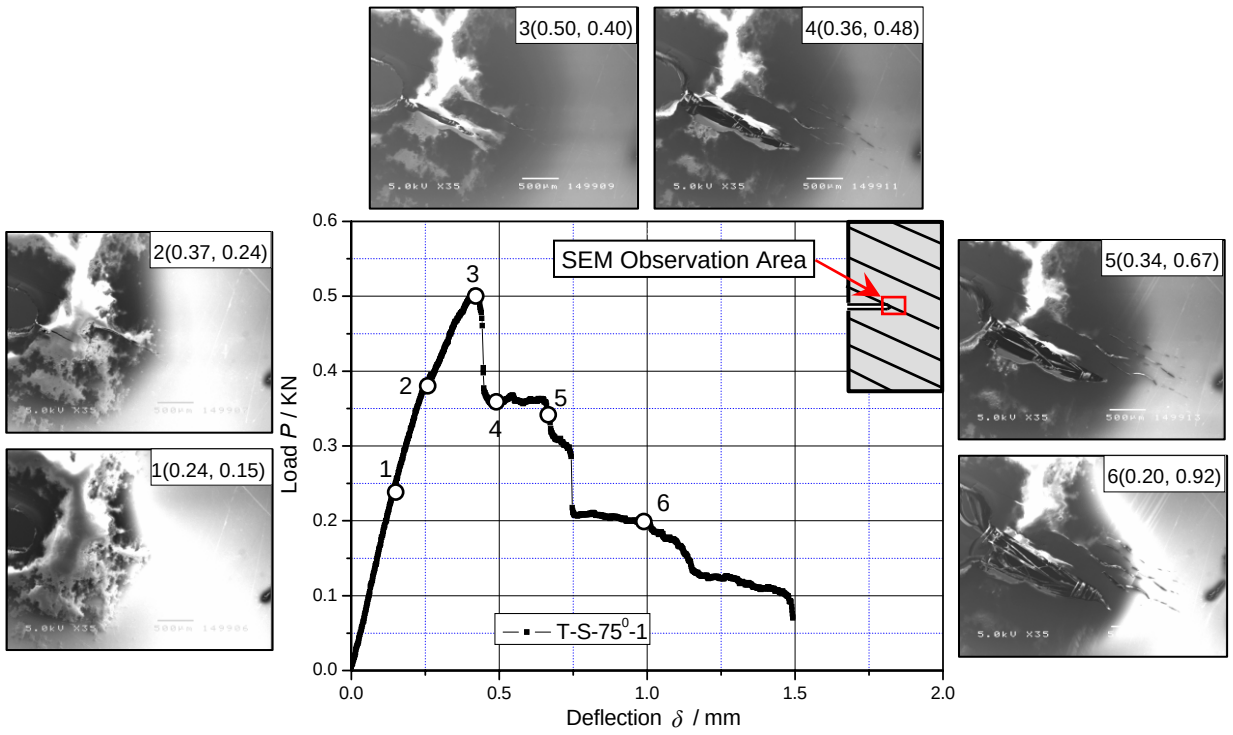
3(0.50, 0.40)
4(0.36, 0.48)
2(0.37, 0.24)
1(0.24, 0.15)
SEM Observation Area
5(0.34, 0.67)
6(0.20, 0.92)
Load P / KN
Deflection δ / mm
T-S-75⁰-1

(f)

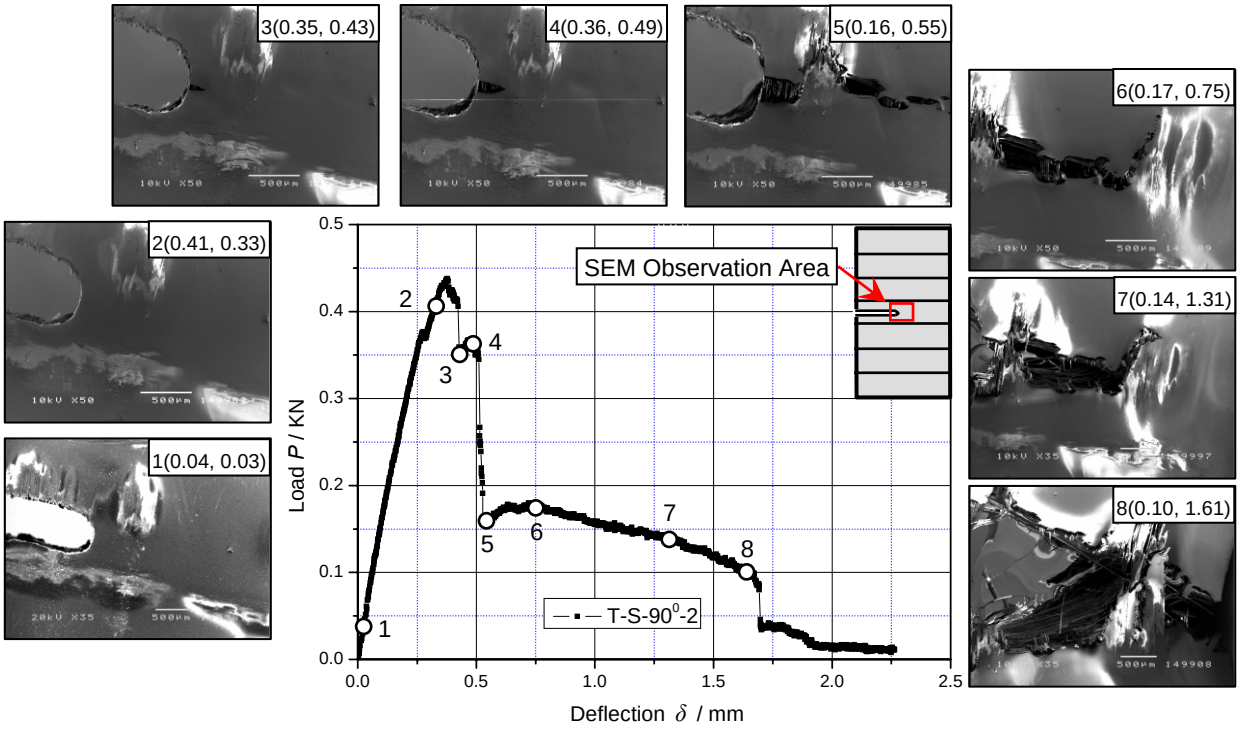

(g)

Figure 9 *SEM photos at different loads in load-deflection (P-δ) curves*.
(a) θ=0^0; (b) θ=15^0; (c) θ=30^0; (d) θ=45^0; (e) θ=60^0; (f) θ=75^0; (g) θ=90^0
Note: numbers at the top-right corner of SEM photos denote the photo number and the corresponding load (kN) and deflection (mm)

3.2 Effect of orientation angels of fibers on fracture modes

We suggest a simple mechanical modelling approach to the effects of orientation angles of fibers on mechanical parameters (Figure 10). The stresses on fibers can be given by

$$\begin{cases} \sigma_n = \sigma_x \sin^2\theta \\ \sigma_t = \sigma_x \sin\theta\cos\theta \end{cases} \tag{9}$$

where σ_n is the normal stress on fibers, governing the breaking of interface between matrix and fiber, σ_t is the shear stress on fibers, governing the fiber damage and failure.

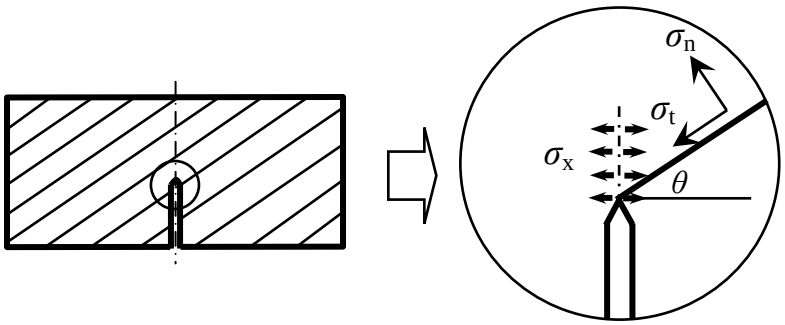

Figure 10 *Schematic view of stress on fiber*.

Equation (9) shows that at lower level of orientation angles of fibers, the normal stresses on fibers are relatively lower. It is the reason why almost no fracture in the matrix occurs at the

notch tip in the cases of lower orientation angles of fibers in the vicinity of peak loads (as shown in Figure 9a, b). In the cases of higher orientation angles, a higher normal stress leads to cracks developing easily and mostly along the interface between the matrix and the fibers (as shown in Figure 9d, e, f, g). In the process, however, the glass fibers seldom fail. In view of the facts that failure stress of glass fibers is much higher than the matrix [8-12], this phenomenon should be reasonable.

In addition, as shown in Figure 9, a further development of a fracture leads to a stress drop in *P-δ* curves. The stress drop increase with the orientation angles of fibers, namely, a larger orientation angle of fibers results in a higher stress drop (Figures 9d, e, f, g). A stress drop usually reflects a rapid development of crack. As a result, if fibers are ideally parallel to the applied load direction (*i.e.*, highest normal stress as shown in Figure 10), the crack develops at the highest speed among all the cases.

4. Conclusions

The effect of the orientation of fibers in unidirectional glass fiber reinforced polymer (GFRP) composites on the damage mechanisms and strength of composites has been investigated experimentally. It was shown that the orientation angles of fibers play an important role in the mechanical behaviour of GFRP composite. The highest strength and stiffness of composites under three-point bending loading are observed when the loading direction is perpendicular to the fiber orientation. The peak strengths, elastic strengths and elastic modulus of GFRP composite decease with the orientation angles of fibers almost linearly. Moreover, SEM photos taken at different loads are used to characterize the meso-scale structure change in the GFRP composite. It is shown that, in the vicinity of peak load, a continuous loading leads to a crack in the matrix first and then causes a fracture along the interface between the matrix and the fibers. Crack propagation path and stress drop are strongly dependent on the orientation angle of fibers.

References

1. G. A. Cooper. The structure and mechanical properties of composite materials. Review of Physics in Technology 2, 1971, 49-91
2. A. G. Evans. Design and life prediction issues for high-temperature engineering ceramics and their composites. *Acta Materialia*, 1997, 45(1): 23-40
3. B. F. Sørensen, and T. K. Jacobsen. Large-scale bridging in composite: R-curves and bridging laws. *Composites Part A*, 1998, 29(A): 1443-1541
4. T. K. Jacobsen, and B. F. Sørensen. Model I intra-laminar crack growth in composite – modeling of R-curves from measured bridging laws. *Composites Part A*, 2001, 32: 1-11
5. B. Budiansky, and N A. Fleck. Compressive failure of fibre composites. *Journal of the Mechanics and Physics of Solids*, 1993, 41(1): 183-211
6. H. T. Hahn, and J. G. Williams. Compressive failure mechanisms in unidirectional composites. NASA TM 85834, 1984
7. J. S. Stölken, and A. G. Evans. A microbend test method for measuring the plasticity length scale. *Acta Materialia*, 1998, 46(14): 5109-5115
8. L. Mishnaevsky Jr. *Computational Mesomechanics of Composites*. John Wiley and Sons, 2007, 293 pp
9. S. Feih, A. Thraner, and H. Lilholt. Tensile strength and fracture surface characterisation of sized and unsized glass fibers. *J of Materials Science*, 2005, 40: 1615 – 1623
10. R. F. Gibson. Dynamic mechanical behavior of fiber-reinforced composites: Measurement and analysis. *J. Compos. Mater.*, 1976, 10: 325–341
11. L. Tevet-Deree. The Dynamic Response of Composite Materials with Viscoelastic Constituents, MsS Thesis, BGU, 2003
12. J. M. L. dos Reis. Mechanical characterization of fiber reinforced Polymer Concrete. *Materials Research*, 2005, 8(3): 357-360